Carbon 116 (2017) 139–144

Contents lists available at ScienceDirect

Carbon

journal homepage: www.elsevier.com/locate/carbon

Thermal transport in graphene with defect and doping: Phonon modes analysis

Shiqian Hu [a, b, c], Jie Chen [a, b, c, *], Nuo Yang [d, e], Baowen Li [f, **]

[a] Center for Phononics and Thermal Energy Science, School of Physics Science and Engineering, Institute for Advanced Study, Tongji University, Shanghai, 200092, People's Republic of China
[b] China–EU Joint Lab for Nanophononics, School of Physics Science and Engineering, Tongji University, Shanghai, 200092, People's Republic of China
[c] Shanghai Key Laboratory of Special Artificial Microstructure Materials and Technology, School of Physics Science and Engineering, Tongji University, Shanghai, 200092, People's Republic of China
[d] State Key Laboratory of Coal Combustion, Huazhong University of Science and Technology (HUST), Wuhan, 430074, People's Republic of China
[e] Nano Interface Center for Energy (NICE), School of Energy and Power Engineering, Huazhong University of Science and Technology (HUST), Wuhan, 430074, People's Republic of China
[f] Department of Mechanical Engineering, University of Colorado, Boulder, CO, 80309, USA

ARTICLE INFO

Article history:
Received 20 November 2016
Received in revised form
23 January 2017
Accepted 27 January 2017
Available online 30 January 2017

ABSTRACT

The effects of defect and isotopic doping with different ratios on the thermal conductivity of graphene are investigated by using non-equilibrium molecular dynamics simulations and normal mode analysis method. In contrast to the persisted size dependent thermal conductivity in the pristine graphene, thermal conductivity of defected graphene quickly saturates when the size is greater than 100 nm. Similar to the pristine graphene, we find the thermal conductivity of defected and doped graphene follows $\sim T^{-\alpha}$ behavior, and the power exponent α is sensitive to the defect and doping ratio. The spectral phonon relaxation time and normalized accumulation thermal conductivity with respect to the phonon mean free path (MFP) reveal that the long-MFP phonon modes are strongly suppressed in the defected and doped graphene, resulting in the suppressed size dependence and the weaker temperature dependence of the thermal conductivity compared to the pristine graphene. The phonon modal analysis in our work establishes a deep understanding of the defect and doping effects on the thermal transport in graphene, which would provide effective guidance to the graphene-based phonon engineering applications.

1. Introduction

The continuous miniaturization of electronic devices results in tremendous escalation in power density, causing severe thermal challenges in the integrated circuit chips. As a novel two-dimensional material, graphene has attracted immense investigations in the past decade due to various fascinating physical properties, such as the high charge mobility [1,2], the superior thermal conductivity [3,4], the optical transparency [5], and strong mechanical strength [6]. In particular, the superior thermal conductivity of graphene (exceeding ~ 3000 W/m-K near room temperature [4]) has triggered growing efforts to develop graphene based nanomaterials [7–12] to address the thermal management issues in the next generation electronic devices.

In the low-dimensional materials, one intriguing phenomenon is that the Fourier's law of heat conduction is violated [13,14], leading to the anomalous heat diffusion [15] and size-dependent thermal conductivity in such systems. The thermal conductivity diverges with the length of system as $\kappa \sim L^{\beta}$ in one-dimensional systems [14,16], while the logarithmic divergence of the thermal conductivity $\kappa \sim \log(L)$ was observed in the two-dimensional nonlinear lattices [17].

The superior thermal conductivity relies on the structural perfection of the graphene. However, the defects are produced inevitably during the experimental process of sample preparation [18,19] and measurement [20], which motivates theoretical works to investigate the effect of defect on the thermal transport [21–25].

* Corresponding author. Center for Phononics and Thermal Energy Science, School of Physics Science and Engineering, Institute for Advanced Study, Tongji University, Shanghai, 200092, People's Republic of China.
** Corresponding author. Department of Mechanical Engineering, University of Colorado, Boulder, CO, 80309, USA.
E-mail addresses: jie@tongji.edu.cn (J. Chen), Baowen.Li@Colorado.Edu (B. Li).

http://dx.doi.org/10.1016/j.carbon.2017.01.089
0008-6223/

For instance, Haskins et al. [14] investigated the influence of different types of defects, and observed substantial reduction in the thermal conductivity of graphene (κ_G) by all forms of defects. Zhang et al. [22] found extremely low κ_G (~3 W/m-K) can be achieved with around 8% vacancy defects. Tan et al. [25] found the effect of the pentagon-heptagon defect on the thermal conduction is stronger in the armchair graphene nanoribbon than the zigzag counterpart. Although extensive efforts have been made to investigate the defect effect on the reduction of κ_G, the impacts of defect on the size dependence and temperature dependence of κ_G has not been systematically investigated yet. In particular, the underlying physical mechanisms in the view of spectral phonon information are still lacking.

In this work, using non-equilibrium molecular dynamics simulations (NEMD), the effect of defect/doping with different ratios on the κ_G is investigated. Moreover, using the normal mode analysis (NMA) method, we calculate the spectral phonon relaxation time of the pristine graphene and defected/doped graphene, respectively. Furthermore, by analyzing of the normalized accumulative thermal conductivity with respect to the phonon mean free path (MFP), we reveal the underlying physical mechanism of the suppressed size dependence and the weak temperature dependence of thermal conductivity in the defected (κ_{DeG}) and doped (κ_{DoG}) graphene.

2. Models and simulation methods

NEMD simulations in this paper are performed using LAMMPS package [26] with the optimized Tersoff [27] potential describing the covalent bonding interaction between carbon atoms in graphene. As shown in Fig. 1(a), the point defects are introduced by randomly removing a carbon atom in graphene, making sure two point defects are not connected with each other as neighboring atoms. The periodic and fixed boundary conditions are used in the width and length direction (Fig. 1(a)), respectively. The time step is set as 0.5 fs.

In order to establish a temperature gradient, the atoms at two ends (six layers) are coupled with Langevin heat bath [28] at temperature T_L and T_R, respectively. In our simulations, we set $T_L = T_0\ (1 + \Delta)$ and $T_R = T_0\ (1 - \Delta)$, where T_0 is the average temperature and Δ is the normalized temperature difference. To study the temperature dependence, we vary T_0 from 300 K to 800 K and fix $\Delta = 0.03$. Fig. 1(b) shows a typical temperature profile of the defected graphene at 300 K. The temperature gradient is obtained by the linear fitting to the local temperature, excluding the temperature jumps at the two ends. The thermal conductivity (κ) is calculated based on the Fourier's Law,

$$\kappa = -\frac{J}{\nabla T}, \tag{1}$$

where ∇T and J is, respectively, the temperature gradient and the heat flux. The heat flux is computed as the energy transported across unit area per unit time. The cross area of graphene is defined as the width (W) multiplied by the inter-layer thickness of graphite ($D = 0.335$ nm). To compute thermal conductivity, NEMD simulations are performed for 10 ns after the system reaching the steady state. The results presented here are averaged over 6 independent simulations with different initial conditions, and the error bar is obtained from the standard deviation of different runs.

3. Results and discussion

3.1. Thermal conductivity

We first study the size dependence of thermal conductivity in the defected graphene. The width of graphene is chosen as 5 nm, which is found to be sufficiently large (details shown in Supplementary Information Fig. S1) to remove the numerical size effect due to the periodic boundary condition used in the width direction. Along the heat conduction (longitudinal) direction, the physical size effect occurs due to the unique nature of two-dimensional system: thermal conductivity increases with the length (L) of graphene as $\log(L)$ in the pristine graphene (inset of Fig. 2), which has been recently confirmed in the experimental study [29] with sample size on the order of 1 μm. In contrast, we find the length dependence is strongly suppressed in the defected graphene: κ_{DeG} is independent on the system size when the length is greater than 100 nm. This result indicates that the defect is a crucial factor that can eliminate the intrinsic logarithm-divergence of κ_G in realistic samples in experiment. Similar suppression of the size dependence has also been reported in the defected CNT [30].

Moreover, due to the Umklapp phonon-phonon scattering at high temperature, thermal conductivity of crystalline materials decreases with the increasing of temperature as$T^{-\alpha}$. In bulk systems where the phonon-phonon scattering is the dominant scattering mechanism, the temperature dependence follows the Slack relation [31], namely, the power exponent α equals 1. We find in our simulation that the boundary scattering plays a significant role when the length is small, leading to the increase of α with L in the pristine graphene (details shown in Supplementary Information Fig. S2(b)), which is consistent with the previous works [30,32]. In this study, as we mainly focus on the relative effect of defect/doping on the temperature dependence of κ_G, we fix the length L as 125 nm in the following simulations.

The temperature dependence of thermal conductivity for the pristine and defected graphene is compared in Fig. 3(a)). The defect ratio is defined as N_{DeG}/N_G, where N_{DeG} and N_G are the number of removed atoms and the total number of atoms in pristine graphene, respectively. The defect ratio varies from 0.03% to 0.5%. Due to the Umklapp phonon–phonon scattering, both κ_G and κ_{DeG} follow the temperature dependence as ~$T^{-\alpha}$. However, compared to the pristine graphene (α is 0.89 when $L = 125$ nm), the power exponent α is significantly decreased in the defected graphene, namely, the weaker temperature dependence. Furthermore, we find α decreases monotonically with the increase of defect ratio (Fig. 3(b)). At the same temperature, κ_{DeG} is significantly reduced compared to κ_G, and decreases monotonically with the defect ratio increasing from 0.03% to 0.5% (Fig. 3(c)). For instance, κ_{DeG} is reduced to 10% of κ_G when the defect ratio is 0.5% at 300 K, which is consistent with the previous work [22]. At high defect ratio, previous theoretical works [22,23] found thermal conductivity of defected graphene saturates with the defect ratio, which has been confirmed by the recent experimental study [33].

3.2. Spectral phonon analysis

In order to understand the underlying physical mechanism for the suppressed size dependence and weak temperature dependence of κ_{DeG}, we perform the spectral phonon analysis for both pristine and defected graphene by using the NMA method. In this formulism, the normal mode velocities are calculated as [34]

$$\dot{q}_{\mathbf{k},p}(t) = \sum_{\alpha}^{3}\sum_{j}^{n}\sum_{l}^{N}\sqrt{\frac{m_j}{N}}\dot{u}_{\alpha}^{l,j}(t)e_{j,\alpha,\mathbf{k},p}^{*}exp\left(-i\mathbf{k}\cdot\mathbf{r}_0^{l,j}\right), \tag{2}$$

where $\mathbf{k}$ is the wave vector, p is the phonon polarization branch, m_j is the atomic mass, N is the total number of unit cells, $\dot{u}_{\alpha}^{l,j}$ is the velocity of the α^{th} component of the jth atom in the lth unit cell which is dumped in MD simulations, $\mathbf{r}_0^{l,j}$ is the equilibrium position

of the atom and $e^{*}_{j,\alpha,\mathbf{k},p}$ is the conjugate of the eigenvector for the jth atom in a specific phonon mode. The phonon dispersion and the eigenvectors are computed by the General Utility Lattice Program (GULP) [35]. In the calculations, we assume the defected graphene has the same phonon dispersion as the pristine graphene, which is a reasonable assumption that has been confirmed in the previous works [23,36]. The power spectrum of $\dot{q}_{\mathbf{k},p}(t)$ is then evaluated as

$$\Phi_{\mathbf{k},p}(\omega) = \left| \int \dot{q}_{\mathbf{k},p}(t) e^{i\omega t} dt \right|^2. \quad (3)$$

To obtain the phonon relaxation time, the power spectrum $\Phi_{\mathbf{k},p}(\omega)$ is fitted with the Lorentz function as

$$\Phi_{\mathbf{k},p}(\omega) = \frac{A_{\mathbf{k},p}}{\left(\omega - \omega^{\alpha}_{\mathbf{k},p}\right)^2 + \Gamma^2_{\mathbf{k},p}}, \quad (4)$$

where $A_{\mathbf{k},p}$, $\omega^{\alpha}_{\mathbf{k},p}$ and $\Gamma_{\mathbf{k},p}$ are the fitting parameters. Here $\omega^{\alpha}_{\mathbf{k},p}$ is the anharmonic phonon frequency, and the phonon relaxation time is equal to $1/(2\Gamma_{\mathbf{k},p})$. To evaluate the mode contribution to thermal conductivity, the spectral thermal conductivity is calculated by using the kinetic theory

$$\kappa_{\mathbf{k},p} = \frac{1}{V} v^2_{\mathbf{k},p} C_{\mathbf{k},p} \tau_{\mathbf{k},p}, \quad (5)$$

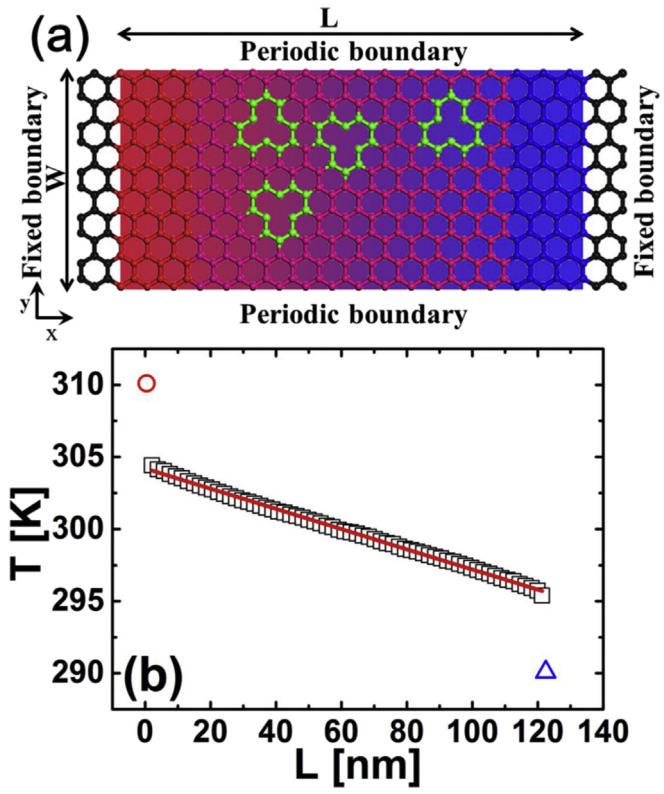

Fig. 1. Simulation setup. (a) Schematic picture of the graphene with randomly distributed point defects. The fixed boundary condition is used along the length (L) direction, while the periodic boundary condition is used along the width (W) direction. (b) The typical temperature profile of the defected graphene at 300 K. The size of the simulation domain is $L = 125$ nm and $W = 5$ nm. Linear fitting is performed to obtain the temperature gradient. The circle and the triangle denote the temperature of the heat source and heat sink, respectively, while the square draws the non-equilibrium local temperature for regions not attached to the heat bath. (A colour version of this figure can be viewed online.)

where V is the volume of the simulation cell, $C_{\mathbf{k},p}$ is the specific heat, $v_{\mathbf{k},p}$ is the group velocity and $\tau_{\mathbf{k},p}$ is the phonon relaxation time. For both the pristine and defected graphene, the spectral phonon relaxation time and the normalized accumulation thermal conductivity with respect to the phonon MFP are computed along the ΓM direction (see Supplementary Information Fig. S3 for details).

The frequency dependent phonon relaxation time for three acoustic branches in the pristine graphene and defected graphene are compared in Fig. 4(a–c). In the pristine graphene, the zone-center low frequency phonons have large relaxation time on the order of 100 ps, consistent with the previous calculation [37]. When the point defects are introduced, the relaxation time for majority phonons is reduced compared to the pristine case. Moreover, there exists a further reduction of the relaxation time when the defect ratio changes from 0.1% to 0.5%. This trend is *qualitatively* consistent with the prediction from the analytical model for the vacancy defect scattering rate (τ^{-1}) defined as [38,39]

$$\tau^{-1} \propto \frac{\pi}{2} f\, \omega^2 g(\omega) \quad (6)$$

where f is the defect/doping ratio, and $g(\omega)$ is the phonon density of states. Based on Eq. (6), the phonon relaxation time τ will decrease with the increase of the defect/doping ratio f. We fit our simulation data with a power law function, and the phonon relaxation time in our work follows $\tau \sim \omega^{-1.1}$ for the defect ratio of 0.5% (see Fig. S7 in supplementary information). The analytical model [38] predicts the defect induced phonon relaxation time follows $\tau \sim \omega^{-4}$ by assuming Debye model $g(\omega) \sim \omega^2$. However, the ZA phonon in graphene has a parabolic dispersion, which deviates significantly from the assumption on the linear dispersion used in the Debye model. In addition, the analytical model only considered impurity atoms perturbation from the mass difference and bond difference [36,38]. However, for the point-defect case, the missing linkages caused by the removable atoms could not be neglected [39]. These factors may be responsible for the discrepancy between the analytical model and our simulation results.

The results in Fig. 4(a–c) show that the low frequency phonons, which have long MFP and contribute most to the thermal conductivity, are strongly suppressed by the defect scattering. To make this point more clear, we show in Fig. 4(d) the normalized accumulative thermal conductivity with respect to phonon MFP for

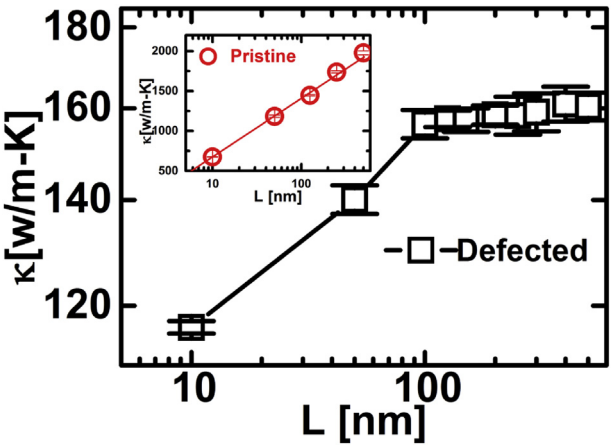

Fig. 2. The length dependence of thermal conductivity in the pristine graphene and defected graphene at 300 K. The defect ratio is fixed as 0.5%, and the error bars are standard deviations of 6 MD simulations with different initial conditions. (A colour version of this figure can be viewed online.)

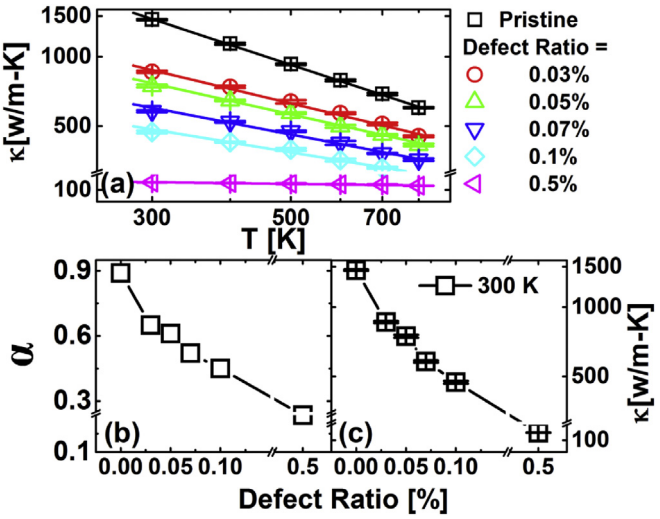

Fig. 3. Effects of the point defect on thermal conductivity of graphene. (a) Log-log plot for the temperature dependence of thermal conductivity in pristine graphene and defected graphene with different defect ratios, showing a $T^{-\alpha}$ behavior. The symbols are simulation results and the lines are the linear fitting lines. The error bars of thermal conductivity are standard deviations of 6 MD simulations with different initial conditions. (b) The power exponent α with respect to the different defect ratios. (c) Thermal conductivity of the pristine graphene and defected graphene with different defect ratios at 300 K. (A colour version of this figure can be viewed online.)

both pristine and defected graphene. We find phonons with MFP larger than 100 nm contribute ~90% of the thermal conductivity in the pristine graphene, consistent with the previous work [36]. When the defects are introduced, the normalized accumulative thermal conductivity curve shifts to the short-MFP end. And a further shift is observed in the defected graphene as the defect ratio increases from 0.1% to 0.5%. If we define dominant phonons as those phonons with accumulative contribution to thermal conductivity in between 10% and 90%, then the dominant phonon MFP is 300–1100 nm for the pristine graphene. This value changes to 100–700 nm and 40–200 nm, respectively, for 0.1% and 0.5% defected graphene. This result clearly indicates the strong suppression of the long-MFP phonons by the defect scattering.

For the pristine graphene, Nika et al. [40] found that the size-dependent thermal conductivity stems from the ballistic transport of phonons with extremely long wavelength (low-frequency). As the size increases, more low-frequency phonons are excited and contribute to thermal transport, leading to a size-dependent behavior. However, when the defects are introduced, the long-MFP (low-frequency) phonons are suppressed significantly (shown in Fig. 4), giving rise to the suppressed size-dependence. This behavior is consistent with the previous finding [41] that the size-dependence is significantly suppressed when the pristine graphene is supported on the amorphous SiO_2 substrate, due to the additional substrate scattering.

For the crystalline solids, McGaughey and Kaviany [42,43] found that the phonons with long MFP are responsible for the temperature dependent thermal conductivity, while the contribution from short-MFP phonons to thermal conductivity is temperature independent. Since the long-MFP phonons are strongly scattered by the defects, their contributions to total thermal conductivity are significantly reduced compared to the pristine graphene, leading to the weaker temperature dependence of thermal conductivity. When the defect ratio increases, the long-MFP phonons are further suppressed, and thus the power exponent α decreases correspondingly. This is the physical origin for the weaker temperature dependence in defected graphene.

So far, we have discussed the size and temperature dependence of thermal conductivity in the defected graphene and the underlying physics. Another approach that has been widely used to control the thermal transport in solids is the doping [28,44] [45]. To this end, we simulate the thermal transport in the isotopically doped graphene, and find the similar behavior of reduced phonon relaxation time and weaken temperature dependence of thermal conductivity in the doped graphene (details shown in Supplementary Information Fig. S4 and Fig. S5). To quantitatively compare the effects of defect and doping on thermal transport, we replace the same amount of graphene atoms (0.5%) with the point defect and ^{13}C isotope, respectively, and compute their thermal transport properties correspondingly. With 0.5% doping, only the relaxation time of some high frequency phonons is slightly reduced compared to the pristine case, while the relaxation time of the zone-center phonons that have long MFP remains intact (Fig. 5(a–c)). With the same amount of defect, the relaxation time of majority phonons, including the zone-center phonons, is further reduced compared to the doping case. As a result, the normalized accumulative thermal conductivity curve for the doped graphene is close to that of the pristine graphene, while an obvious shift towards the short-MFP end is observed for the defected graphene (Fig. 5(d)). Therefore, we find the defect has a stronger impact than the doping on the thermal transport given the same defect/doping ratio.

In the experimental synthesis of graphene, the sample quality is usually difficult to control, and the defects can be commonly produced during the experimental process of sample preparation and measurement. Our results show that defect scattering can strongly suppress the low frequency phonons which have long MFP and are responsible for the length dependence, making it challenging to experimentally observe the logarithmic length dependence of thermal conductivity in graphene. Furthermore, our results demonstrate that the temperature dependence of thermal

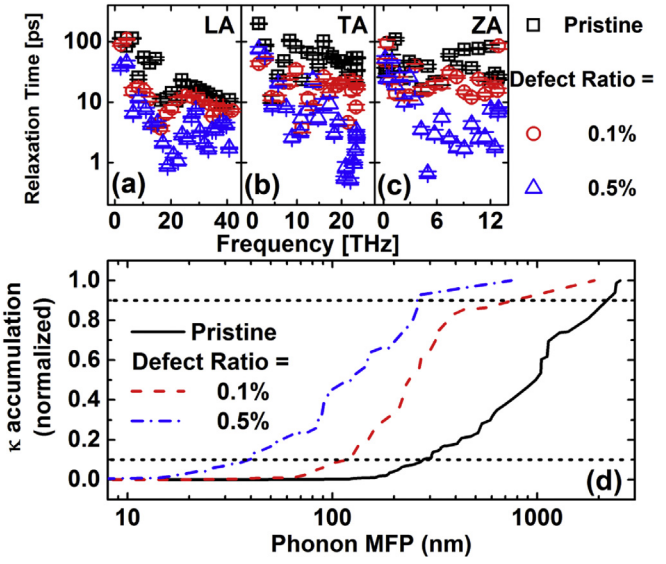

Fig. 4. The effects of defect on thermal transport properties of graphene. Phonon relaxation time for (a) longitudinal acoustic (LA), (b) transverse acoustic (TA), and (c) flexural acoustic (ZA) branches along the ΓM direction in both pristine and defected graphene. The relaxation time in the defected graphene is significantly reduced compared to the pristine case. The error bars are obtained from the fitting errors of the power spectrum $\Phi_{\mathbf{k}p}(\omega)$. (d) The normalized accumulative thermal conductivity of the pristine graphene and defected graphene with respect to the phonon mean free path. The curves shift to the short-MFP end as the defect ratio increases. (A colour version of this figure can be viewed online.)

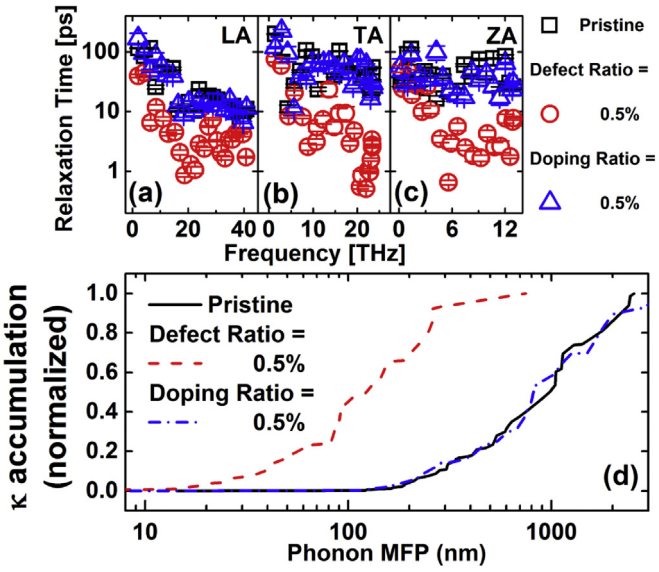

Fig. 5. Comparison of the effects of defect and doping on thermal transport properties of graphene. Phonon relaxation time of LA (a), TA (b) and ZA (c) along the ΓM direction in the pristine graphene and defected/doped graphene. The defect/doping ratio is fixed as 0.5%. The error bars are obtained from the fitting errors of the power spectrum $\Phi_{\mathbf{k},p}(\omega)$. (d) The normalized accumulative thermal conductivity of the pristine graphene and defected/doped graphene (0.5% defect/doping ratio) with respect to the phonon mean free path. (A colour version of this figure can be viewed online.)

conductivity in graphene can be continuously tuned by the defect/doping ratio. This can create novel materials with grading and piecewise temperature dependent thermal conductivity, which can have promising application as the high-efficiency thermal rectifier [46]. In addition, we believe a clear understanding of the spectral phonon information in the defected/doped graphene could provide valuable insights to some phononic applications which require the precise modulation of phonons with specific frequency, such as phonon nanocapacitor [47] and thermal cloaking [48,49].

4. Conclusions

In summary, we investigated the effects of defect and doping on the thermal conductivity in graphene through molecular dynamics simulations. In contrast to the persisted size dependent thermal conductivity in pristine graphene, thermal conductivity of the defected graphene is found to saturate when the length is longer than 100 nm. Moreover, we find thermal conductivity in defect/doped graphene follows $T^{-\alpha}$ temperature dependence, and the power exponent decreases monotonically with the defect/doping ratio. The spectral phonon analysis reveals that the long-MFP phonons are strongly suppressed by the defect scattering, giving rise to the suppressed size effect and the weaker temperature dependence. For the same concentration, the defect scattering is found to have a stronger impact than the isotopic scattering on the thermal transport in graphene. Our study provides valuable insights to the phononic applications based on the defect engineering.

Acknowledgements

This project is supported in part by the grants from the National Natural Science Foundation of China: 51506153, 11334007, and 51576076. J. C. acknowledges support from the National Youth 1000 Talents Program in China, and the startup grant at Tongji University. The authors thank the National Supercomputing Center in Guangzhou (NSCC-GZ) for the computing resources.

Appendix A. Supplementary data

Supplementary data related to this article can be found at http://dx.doi.org/10.1016/j.carbon.2017.01.089.

References

[1] K.S. Novoselov AKG, S.V. Morozov, D. Jiang, Y. Zhang, S.V. Dubonos, I.V. Grigorieva, A.A. Firsov, Electric field effect in atomically thin carbon films, Science 306 (2004) 666–669.
[2] Y.B. Zhang, Y.W. Tan, H.L. Stormer, P. Kim, Experimental observation of the quantum Hall effect and Berry's phase in graphene, Nature 438 (7065) (2005) 201–204.
[3] A.A. Balandin, S. Ghosh, W. Bao, I. Calizo, D. Teweldebrhan, F. Miao, et al., Superior thermal conductivity of single-layer graphene, Nano Lett. 8 (3) (2008) 902–907.
[4] A.A. Balandin, Thermal properties of graphene and nanostructured carbon materials, Nat. Mater. 10 (2011) 569–581.
[5] R.R. Nair PB, A.N. Grigorenko, K.S. Novoselov, T.J. Booth, T. Stauber, N.M.R. Peres, A.K. Geim, Fine structure constant defines visual transparency of graphene, Science 320 (2008) 1308.
[6] C. Lee XW, J.W. Kysar, J. Hone, Measurement of the elastic properties and intrinsic strength of monolayer graphene, Science 321 (2008) 385–388.
[7] J. Chen, J.H. Walther, P. Koumoutsakos, Covalently bonded graphene-carbon nanotube hybrid for high-performance thermal interfaces, Adv. Funct. Mater. 25 (48) (2015) 7539–7545.
[8] D. Alexeev, J. Chen, J.H. Walther, K.P. Giapis, P. Angelikopoulos, P. Koumoutsakos, Kapitza resistance between few-layer graphene and water: liquid layering effects, Nano Lett. 15 (9) (2015) 5744–5749.
[9] H. Han, Y. Zhang, N. Wang, M.K. Samani, Y. Ni, Z.Y. Mijbil, et al., Functionalization mediates heat transport in graphene nanoflakes, Nat. Commun. 7 (2016) 11281.
[10] J. Chen, J.H. Walther, P. Koumoutsakos, Strain engineering of kapitza resistance in few-layer graphene, Nano Lett. 14 (2) (2014) 819–825.
[11] L.F.C. Pereira, D. Donadio, Divergence of the thermal conductivity in uniaxially strained graphene, Phys. Rev. B 87 (12) (2013) 125424.
[12] J. Chen, J.H. Walther, P. Koumoutsakos, Ultrafast cooling by covalently bonded graphene-carbon nanotube hybrid immersed in water, Nanotechnology 27 (46) (2016) 465705.
[13] C. Chang, D. Okawa, H. Garcia, A. Majumdar, A. Zettl, Breakdown of Fourier's law in nanotube thermal conductors, Phys. Rev. Lett. 101 (7) (2008) 075903.
[14] N. Yang, G. Zhang, B. Li, Violation of Fourier's law and anomalous heat diffusion in silicon nanowires, Nano Today 5 (2) (2010) 85–90.
[15] S. Liu, P. Hanggi, N. Li, J. Ren, B. Li, Anomalous heat diffusion, Phys. Rev. Lett. 112 (4) (2014) 040601.
[16] J.-S. Wang, B. Li, Intriguing heat conduction of a chain with transverse motions, Phys. Rev. Lett. 92 (7) (2004) 074302.
[17] L. Wang, B. Hu, B. Li, Logarithmic divergent thermal conductivity in two-dimensional nonlinear lattices, Phys. Rev. E 86 (4) (2012) 040101.
[18] D. Sen, K.S. Novoselov, P.M. Reis, M.J. Buehler, Tearing graphene sheets from adhesive substrates produces tapered nanoribbons, Small 6 (10) (2010) 1108–1116.
[19] J. Kotakoski, A. Krasheninnikov, U. Kaiser, J. Meyer, From point defects in graphene to two-dimensional amorphous carbon, Phys. Rev. Lett. 106 (10) (2011) 105505.
[20] M.H. Gass, U. Bangert, A.L. Bleloch, P. Wang, R.R. Nair, A. Geim, Free-standing graphene at atomic resolution, Nat. Nanotechnol. 3 (11) (2008) 676–681.
[21] J. Haskins, A. Kınacı, C. Sevik, Hl Sevincli, G. Cuniberti, T. Cagın, Control of thermal and electronic transport in defect-engineered graphene nanoribbons, ACS Nano 5 (5) (2011) 3779–3787.
[22] H. Zhang, G. Lee, K. Cho, Thermal transport in graphene and effects of vacancy defects, Phys. Rev. B 84 (11) (2011) 115460.
[23] F. Hao, D. Fang, Z. Xu, Mechanical and thermal transport properties of graphene with defects, Appl. Phys. Lett. 99 (4) (2011) 041901.
[24] X. Liu, G. Zhang, Y.W. Zhang, Topological defects at the graphene/h-BN interface abnormally enhance its thermal conductance, Nano Lett. 16 (8) (2016) 4954–4959.
[25] S.-H. Tan, L.-M. Tang, Z.-X. Xie, C.-N. Pan, K.-Q. Chen, Effect of pentagon-heptagon defect on thermal transport properties in graphene nanoribbons, Carbon 65 (2013) 181–186.
[26] S. Plimpton, Fast parallel algorithms for short-range molecular dynamics, J. Comp. Phys. 117 (1) (1995) 1–19.
[27] L. Lindsay, D.A. Broido, Optimized Tersoff and Brenner empirical potential parameters for lattice dynamics and phonon thermal transport in carbon nanotubes and graphene, Phys. Rev. B 81 (20) (2010) 205441.
[28] N. Yang, G. Zhang, B. Li, Ultralow thermal conductivity of isotope-doped silicon nanowires, Nano Lett. 8 (1) (2008) 276–280.
[29] X. Xu, L.F. Pereira, Y. Wang, J. Wu, K. Zhang, X. Zhao, et al., Length-dependent thermal conductivity in suspended single-layer graphene, Nat. Commun. 5

(2014) 3689.
[30] C. Sevik, H. Sevincli, G. Cuniberti, T. Cagin, Phonon engineering in carbon nanotubes by controlling defect concentration, Nano Lett. 11 (11) (2011) 4971–4977.
[31] M. Kaviany, Heat Transfer Physics, Cambridge University Press, New York, 2008, p. 212.
[32] S. Hu, M. An, N. Yang, B. Li, Manipulating the temperature dependence of the thermal conductivity of graphene phononic crystal, Nanotechnology 27 (26) (2016) 265702.
[33] H. Malekpour, P. Ramnani, S. Srinivasan, G. Balasubramanian, D.L. Nika, A. Mulchandani, et al., Thermal conductivity of graphene with defects induced by electron beam irradiation, Nanoscale 8 (30) (2016) 14608–14616.
[34] W. Xu, G. Zhang, B. Li, Thermal conductivity of penta-graphene from molecular dynamics study, J. Chem. Phys. 143 (15) (2015) 154703.
[35] J.D. Gale, GULP: a computer program for the symmetry-adapted simulation of solids, J. Chem. Soc. Faraday Trans. 93 (4) (1997) 629–637.
[36] T.L. Feng, X.L. Ruan, Z.Q. Ye, B.Y. Cao, Spectral phonon mean free path and thermal conductivity accumulation in defected graphene: the effects of defect type and concentration, Phys. Rev. B 91 (22) (2015) 224301.
[37] B. Qiu, X. Ruan, Reduction of spectral phonon relaxation times from suspended to supported graphene, Appl. Phys. Lett. 100 (19) (2012) 193101.
[38] C. Ratsifaritana, P. Klemens, Scattering of phonons by vacancies, Int. J. Thermophys. 8 (6) (1987) 737–750.
[39] Z. Ding, Q.-X. Pei, J.-W. Jiang, Y.-W. Zhang, Manipulating the thermal conductivity of monolayer MoS2 via lattice defect and strain engineering, J. Phys. Chem. C 119 (28) (2015) 16358–16365.
[40] D. Nika, S. Ghosh, E. Pokatilov, A. Balandin, Lattice thermal conductivity of graphene flakes: comparison with bulk graphite, Appl. Phys. Lett. 94 (20) (2009) 203103.
[41] J. Chen, G. Zhang, B. Li, Substrate coupling suppresses size dependence of thermal conductivity in supported graphene, Nanoscale 5 (2) (2013) 532–536.
[42] A.J.H. McGaughey, M. Kaviany, Thermal conductivity decomposition and analysis using molecular dynamics simulations. Part I. Lennard-Jones argon, Int. J. Heat. Mass Trans. 47 (8–9) (2004) 1783–1798.
[43] A.J.H. McGaughey, M. Kaviany, Thermal conductivity decomposition and analysis using molecular dynamics simulations: Part II. Complex silica structures, Int. J. Heat. Mass Trans. 47 (8) (2004) 1799–1816.
[44] J.-W. Jiang, J. Lan, J.-S. Wang, B. Li, Isotopic effects on the thermal conductivity of graphene nanoribbons: localization mechanism, J. Appl. Phys. 107 (5) (2010) 054314.
[45] X. Li, J. Chen, C. Yu, G. Zhang, Comparison of isotope effects on thermal conductivity of graphene nanoribbons and carbon nanotubes, Appl. Phys. Lett. 103 (1) (2013) 013111.
[46] S. Hu, M. An, N. Yang, B. Li, A series circuit of thermal rectifiers: an effective way to enhance rectification ratio, Small (2017) 1602726, http://dx.doi.org/10.1002/smll.201602726.
[47] H. Han, B. Li, S. Volz, Y.A. Kosevich, Ultracompact interference phonon nanocapacitor for storage and lasing of coherent terahertz lattice waves, Phys. Rev. Lett. 114 (14) (2015) 145501.
[48] T. Han, X. Bai, D. Gao, J.T.L. Thong, B. Li, C.W. Qiu, Experimental demonstration of a bilayer thermal cloak, Phys. Rev. Lett. 112 (5) (2014) 054302.
[49] T. Han, X. Bai, J.T. Thong, B. Li, C.W. Qiu, Full control and manipulation of heat signatures: cloaking, camouflage and thermal metamaterials, Adv. Mater. 26 (11) (2014) 1731–1734.